Bulletin of Electrical Engineering and Informatics
Vol. 14, No. 6, December 2025, pp. 4208~4221
ISSN: 2302-9285, DOI: 10.11591/eei.v14i6.10877

Designing an A+ LED solar simulator: spectrum optimization and its impact on silicon solar cells

Chaiyant Boonmee[1], Patcharanan Sritanauthaikorn[1], Saichol Chudjuarjeen[2], Paiboon Kiatsookkanatorn[3], Khanittha Wannakam[1], Jeerawan Homjan[4], Kreeta Sukthang[4], Panet Sooksing[5], Napat Watjanatepin[6]

[1]Department of Electrical Engineering, Faculty of Engineering and Architecture, Rajamangala University of Technology Suvarnabhumi, Nonthaburi Campus, Nonthaburi, Thailand
[2]Department of Electrical Engineering, Faculty of Engineering, Rajamangala University of Technology Krungthep, Bangkok, Thailand
[3]Department of Electrical Engineering, Faculty of Engineering and Architecture, Rajamangala University of Technology Suvarnabhumi, Suphanburi Campus, Suphanburi, Thailand
[4]Department of Mechatronics Engineering, Faculty of Engineering and Architecture, Rajamangala University of Technology Suvarnabhumi, Nonthaburi Campus, Nonthaburi, Thailand
[5]Department of Electrical Engineering, Faculty of Engineering, Thonburi University, Bangkok, Thailand
[6]Department of Electrical Engineering, Faculty of Engineering, Bangkokthonburi University, Bangkok, Thailand

Article Info

Article history:

Received Jun 17, 2025
Revised Sep 3, 2025
Accepted Sep 27, 2025

Keywords:

Class A+ spectrum
Light-emitting diode solar simulator
Silicon solar cells
Spectral coverage
Spectral deviation

ABSTRACT

The development of light-emitting diode (LED)-based solar simulators that comply with the updated IEC 60904-9:2020 standard, particularly achieving a Class A+ irradiance spectrum, remains a significant challenge. This necessitates careful consideration of two key spectral quality indicators: spectral deviation (SPD) and spectral coverage (SPC). This study proposes a method to achieve a Class A+ solar simulator spectrum using a minimal number of LED types while optimizing SPD and SPC. It also examines the influence of SPD and SPC on the photogenerated current density (J_{ph}) and short-circuit current density (J_{sc}) of crystalline silicon and multi-crystalline silicon solar cells. By selectively adding ultraviolet (UV) and near-infrared (NIR) LEDs to the original six-type LED configuration, the simulator's spectral performance was enhanced to more closely align with the AM1.5G standard. The configuration incorporating both UV and NIR LEDs demonstrated the highest performance. It achieved an SPC of 97.521% and the lowest SPD at 26.088%. Simulation results confirmed that higher SPC and lower SPD values contribute to reduced errors in the calculated J_{sc} and J_{ph} for both crystalline silicon (c-Si) and multi-crystalline silicon (mc-Si) solar cells. These findings highlight the importance of well-balanced spectral design and demonstrate that accurate spectral simulation is achievable using only essential LED wavelengths.

Corresponding Author:

Patcharanan Sritanauthaikorn
Department of Electrical Engineering, Faculty of Engineering and Architecture
Rajamangala University of Technology Suvarnabhumi, Nonthaburi Campus
217 Nonthaburi Road, Suanyai, Muang, Nonthaburi, 11000, Thailand
email: patcharanan.s@rmutsb.ac.th

1. INTRODUCTION

A solar simulator is a precision lighting instrument designed to replicate both the irradiance and spectral distribution of natural sunlight [1]. It plays a vital role in indoor testing and performance evaluation of solar cells, photovoltaic modules, and other optoelectronic devices sensitive to solar radiation [2]. The

light-emitting diode solar simulator (LSS) typically comprises a large array of light-emitting diodes (LEDs), each emitting at different spectral bands. When combined, these LEDs produce a composite spectrum that closely mimics sunlight. One of the key advantages of such systems is their high degree of spectral tunability [3]. However, this flexibility comes with the challenge of configuring a large number of parameters to achieve an optimal spectral mismatch (SM) [4].

In 2020, the IEC 60904-9 [5] standard was updated with stricter spectral accuracy requirements to improve photovoltaic measurement precision, particularly for advanced solar cell technologies. The revision introduced two new metrics, spectral deviation (SPD) and spectral coverage (SPC), to better assess how well solar simulators, especially LED-based ones, replicate the solar spectrum. These changes enhance the reliability and comparability of solar cell performance testing across different setups.

These recent changes have driven research and development efforts in solar simulators toward the highest benchmark, achieving Class A+ spectral performance, with SPD approaching 0% and SPC reaching the ideal value of 100%. At present, there are only a limited number of published studies on LSS that meet the stringent Class A+ spectral standards outlined in IEC 60904-9:2020, underscoring the significant technical challenges involved in designing and developing such systems. A literature review conducted by the author in 2023, titled light sources and irradiance spectrum of LSS for photovoltaic devices [6], revealed that although the development of LSS has increased substantially since the year 2000, the majority of these systems were designed by the earlier IEC 60904-9:2007 standard [7]. The review also found that existing LSS systems have neither achieved Class A+ irradiance spectrum across the full 300 to 1,200 nm wavelength range, nor provided comprehensive evaluations of SPC and SPD under the new 2020 standard.

To the best of the author's knowledge, only Vosylius *et al.* [8], [9] have developed solar simulator spectra under IEC 60904-9:2020 using LED-only and LED–halogen lamp (HL) configurations. In [8], a Class A+ spectrum was achieved with five LEDs (365 nm, cool white, 740 nm, 850 nm, and 1050 nm), yielding SPC/SPD of 89.1%/65.5%; adding NIR from HL improved these to 97.2%/37.8%. In [9], six LEDs (365 nm, cool white, 740 nm, 850 nm, 940 nm, and 1050 nm) achieved 91.8%/61.1%, further enhanced to 98.2%/39.5% with 405 nm LEDs and HL components.

Although LSS and LED-hybrid solar simulators have achieved promising SPC and SPD values [8], [9], integrating LEDs with HL on a single platform poses three main challenges: i) SM – HL's low energy efficiency generates significant heat, raising the temperature of circuit boards and nearby LEDs, thereby altering their emission spectra and reducing peak photon density [10]; ii) temporal instability – HL's slow warm-up/cool-down causes light intensity fluctuations during start-up or with ambient temperature changes [11]; and iii) non-uniform irradiance – the directional, narrow-band output of LEDs contrasts with HL's broad, omnidirectional emission, leading to localized hot and cool spots on the test surface [12], [13].

Therefore, focusing on the development of an LED-only Class A+ solar simulator can effectively address these three limitations while ensuring compliance with the enhanced spectral accuracy requirements of the IEC 60904-9:2020 standard. Furthermore, there is currently a lack of in-depth investigation into the effects of SPD and SPC on the photocurrent behaviour of solar cells under artificial spectra generated by LED-based light sources. The authors have identified two key research challenges that this work aims to address:

- How can a Class A+ spectrum (with SPC ≥ 98% and SPD ≤ 37%) be achieved using the fewest possible types of LEDs?
- How do SPD and SPC influence the photocurrent and short-circuit current for c-Si and mc-Si solar cells?

The objective of this article is to present a method for simulating a Class A+ solar simulator spectrum using only LED-based light sources, while minimizing the number of LED types required to obtain optimal values of SPD and SPC, without compromising the spectral conformity defined by Class A+ standards. Additionally, the study aims to analyse the impact of SPD and SPC on the photogenerated current density (J_{ph}) and short-circuit current density (J_{sc}) of crystalline silicon (c-Si) and multi-crystalline silicon (mc-Si) solar cells.

The article presents a Class A+ solar simulator using six LED types, including UV and NIR. Spectrum optimization through LED intensity and composition, analyzed with spectrum calculation software [8], [14], shows that improving SPD and SPC significantly reduces J_{sc} and J_{ph} measurement errors in c-Si and mc-Si cells compared to the standard reference spectrum.

2. MATERIAL AND METHOD

The SPC and the SPD parameters, LED characteristics, and solar spectrum are discussed in this section. Spectrum optimization is approached in four distinct cases. The influence of SPD and SPC on the photogenerated current density (J_{ph}) and short-circuit current density (J_{sc}) of c-Si and mc-Si solar cells is also described.

2.1. AM1.5 spectral coverage

The SPC quantifies the extent to which a solar simulator replicates the AM1.5 spectrum across relevant wavelengths. It is calculated as the ratio of the integrated AM1.5 irradiance over wavelengths where the simulator's irradiance exceeds 10% of the AM1.5 value, to the total AM1.5 irradiance within the 300–1,200 nm range [5], as defined by IEC 60904-9:2020. This is computed using (1). A higher SPC value indicates a closer spectral match to natural sunlight [15], which reflects improved simulator accuracy for photovoltaic testing.

$$\text{SPC}=\left(\sum_{E_{SIM}(\lambda)>0.1\times E_{AM1.5}(\lambda)} E_{AM1.5}(\lambda)\cdot\Delta\lambda \,/\, \sum_{300\,nm}^{1200\,nm} E_{AM1.5}(\lambda)\cdot\Delta\lambda\right)\cdot 100\% \quad (1)$$

2.2. AM1.5 spectral deviation

The SPD parameter quantifies the total deviation between the two curves and indicates how closely the spectral irradiance from the solar simulator matches the AM1.5 spectral irradiance [5]. The equation used to calculate the AM1.5 SPD by IEC 60904-9:2020 is given as (2). A lower SPD value indicates that the artificial light spectrum closely matches the AM1.5 spectrum. An SPD value of 0 means that the light spectrum is identical to the AM1.5 spectrum in every aspect.

$$\text{SPD}=\left((\sum_{300\,nm}^{1200\,nm}|E_{SIM}(\lambda)-E_{AM1.5}(\lambda)|\cdot\Delta\lambda)/(\sum_{300\,nm}^{1200\,nm} E_{AM1.5}(\lambda)\cdot\Delta\lambda)\right)\cdot 100\% \quad (2)$$

2.3. Light-emitting diode types and characteristics

This section provides more detailed information about the LEDs used in this study, including their types, characteristics, model numbers, and manufacturers, as summarized in Table 1. Table 1 details the LEDs used, grouped into UV (340 and 365 nm), visible (400–700 nm, using Pc-wLEDs) [2], and NIR (730–1,100 nm), along with their voltage, current, model numbers, and manufacturers (e.g., 340 nm LED, model M340D3, Thorlabs). The proposed spectrum emission (P-SPE), classified as Class A+ per [5], was measured using a spectroradiometer and serves as the study's baseline. Three variants—P-SPE+340 nm, P-SPE+1100 nm, and P-SPE+340 nm+1100 nm—were generated to assess SPC and SPD effects.

Table 1. Models and characteristics of the LEDs

Type	Wavelength (nm)	Forward voltage (V)	Forward current (mA)	Model	Configuration
UV	340	4.6	700	M340D3*	
	365	4.4	700	M365D1*	Proposed spectrum
Visible	400–700	34–38	300	LC-10FS504-A29**	
NIR	730	2.9	1000	M730D3*	
	810	3.6	500	M810D2*	
	880	1.7	1000	M880D2*	
	1000	3–4.5	1050	LC-10IR9-A42**	
	1100	1.2	1000	OCI-490-20 ID1100-XE***	

Remark: *THORLABS [16] **LCFOCUS *** EPIGAP OSA Photonics GmbH [17].

2.4. Baseline spectrum

The baseline spectrum, adapted from [5], was optimized to minimize LED types, using six LEDs: UV (365 nm), Pc-wLEDs (400–700 nm), and NIR (730, 810, 880, and 1,000 nm). Spectral power data from manufacturers (see Table 1). The spectral power data, provided in .xls format, were obtained from the manufacturers' websites [16], [17], while the spectrum data for Pc-wLEDs were derived from spectroradiometer measurements reported in [2]. The spectral power data were calibrated using the spectrum mismatch calculator [14], and the AM1.5G spectrum data, also available in .xls format, can be accessed from the same source. The total irradiance of baseline spectrum was adjusted to meet Class A+ at 1 Sun (1,000 W/m², with 836 W/m² in the 300–1,200 nm range) [8].

Subsequently, the numerical spectral data of both the P-SPE and the AM1.5G reference spectrum were used to calculate the SPC and SPD The calculations were implemented in a spreadsheet using (1) and (2). Additionally, the spreadsheet included commands to compute the SM based on the ratio of spectral power values (W/m²) between the baseline spectrum and the AM1.5G spectrum across six wavelength intervals specified in the IEC 60904-9 standard [5]. The resulting SM values served as indicators to evaluate whether the adjusted LED spectral power met the target Class A+ classification for the LSS spectrum. In this study, the optimized baseline spectrum is referred to as P-SPE, and the corresponding calculated performance parameters are presented in section 3.

2.5. Optimization spectrum

This study proposes a simulation spectrum optimization approach in four distinct cases.

- P-SPE: is the baseline spectrum of the LSS, composed of six types of LEDs, with details described in section 2.4. The simulated P-SPE is located in worksheet 1 of the *.xls* file.
- P-SPE+340: worksheet-2 was generated from worksheet-1 of P-SPE (case 1) to improve SPC in the UV range (300–470 nm). A 340 nm LED was added, while the 365 nm LED power was reduced, adjusting the UV amplitude to ~140.361 W/m². SM was maintained at Class A+, and total irradiance remained 836 W/m² ±2%. Amplitude adjustments were applied via multiplication factors to the spectrum power data from section 2.4, resulting in the P-SPE+340 simulation outcomes presented in section 3.1.
- P-SPE+1100: worksheet-3 was generated from case 1 to extend the NIR range (919–1200 nm) by adding a 1100 nm LED and reducing the 1000 nm LED irradiance. Amplitude adjustments were applied via multiplication factors to achieve a total irradiance of ~139.89 W/m² while maintaining Class A+ SM across all six wavelength bins. These modifications resulted in the P-SPE+1100 simulation outcomes showed in section 3.1
- P-SPE+340+1100: worksheet-4 was generated from case 1 by adding 340 nm and 1,100 nm LEDs to achieve full wavelength coverage (300–470 nm and 919–1,200 nm). The amplitudes of UV and NIR LEDs were adjusted via spreadsheet simulation, and the SM was verified across all relevant bins to ensure Class A+ compliance. The resulting P-SPE+340+1100 simulation outcomes are revealed in section 3.1.

2.6. Simulation J_{sc} and J_{ph} on silicon solar cell

To simulate J_{sc} and J_{ph}, the c-Si (IBC, SunPower Gen3) and mc-Si (PERL, UNSW honeycomb mc-Si) EQE curves were selected from the spectrum mismatch calculator library [14] as representative of widely used commercial cells. The c-Si IBC cell reflects high-efficiency monocrystalline technology, while the mc-Si PERL cell represents typical industrial multi-crystalline modules. These selections ensure that the simulation results are relevant to real-world photovoltaic performance.

These cells were chosen for their broad 400–1,000 nm spectral response, which closely matches the AM1.5G spectrum. The simulation (Figure 1) designates Spectrum A as AM1.5G and Spectrum B as the proposed spectrum (e.g., P-SPE variants), covering 300–1,200 nm.

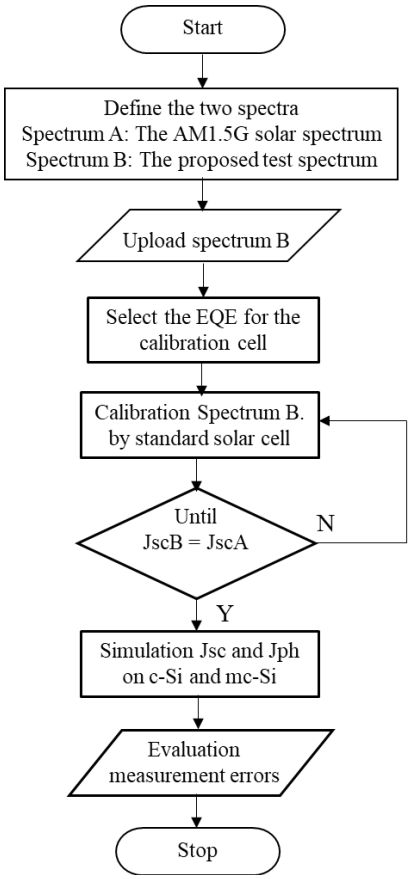

Figure 1. Simulation process of spectrum mismatch calculator on J_{sc} and J_{ph} of c-Si and mc-Si

An external quantum efficiency (EQE) curve is selected for a calibration cell to normalize the intensity of Spectrum B. The proposed spectrum is uploaded and scaled until the simulated short-circuit current density under Spectrum B (J_{scB}) matches that of AM1.5G (J_{scA}), ensuring equivalent irradiance power for the calibration cell. Subsequently, EQE profiles of the test cells—c-Si and mc-Si [18]—are used to simulate their J_{sc} and J_{ph}. The software integrates each spectrum with the cell's EQE to compute J_{scA}/J_{phA} (AM1.5G) and J_{scB}/J_{phB} (proposed spectrum), followed by calculating the relative error between them. As the simulations in this study were not replicated, the error analysis shown in the relative error graphs is derived from the uncertainties of the simulation instruments and the measured original spectrum irradiance, which are reported as ±5%.

3. RESULTS AND DISCUSSION

In this section, the results of the simulation show the spectrum and evaluation of SM, SPD, and SPC. The impact and effect of SPD and SPC on J_{sc} and J_{ph} of c-Si and mc-Si solar cells are also discussed. They are presented in 4 cases.

3.1. Simulation results of spectrum and evaluation of SM, SPD, and SPC

This section presented the results of the spectrum optimization and the evaluation of SM, SPD, and SPC. The analysis began with the P-SPE or baseline spectrum generated from six types of LEDs (Figure 2(a)), which satisfied Class A+ requirements as defined by IEC 60904-9:2020. Subsequently, the spectrum was optimized by adding the spectral contributions of a single UV LED (Figure 2(b)), a single NIR LED (Figure 2(c)), and a combination of both UV and NIR LEDs (Figure 2(d)). The objective is to enhance the SPD and SPC performance of the P-SPE while maintaining compliance with Class A+ criteria. To ensure simplicity and practicality, only one type of LED is added for each wavelength region (UV and NIR), avoiding the use of halogen-lamp-based NIR sources as previously justified in the introduction. The detailed analysis and evaluation results for each optimized configuration were provided in the following subsections.

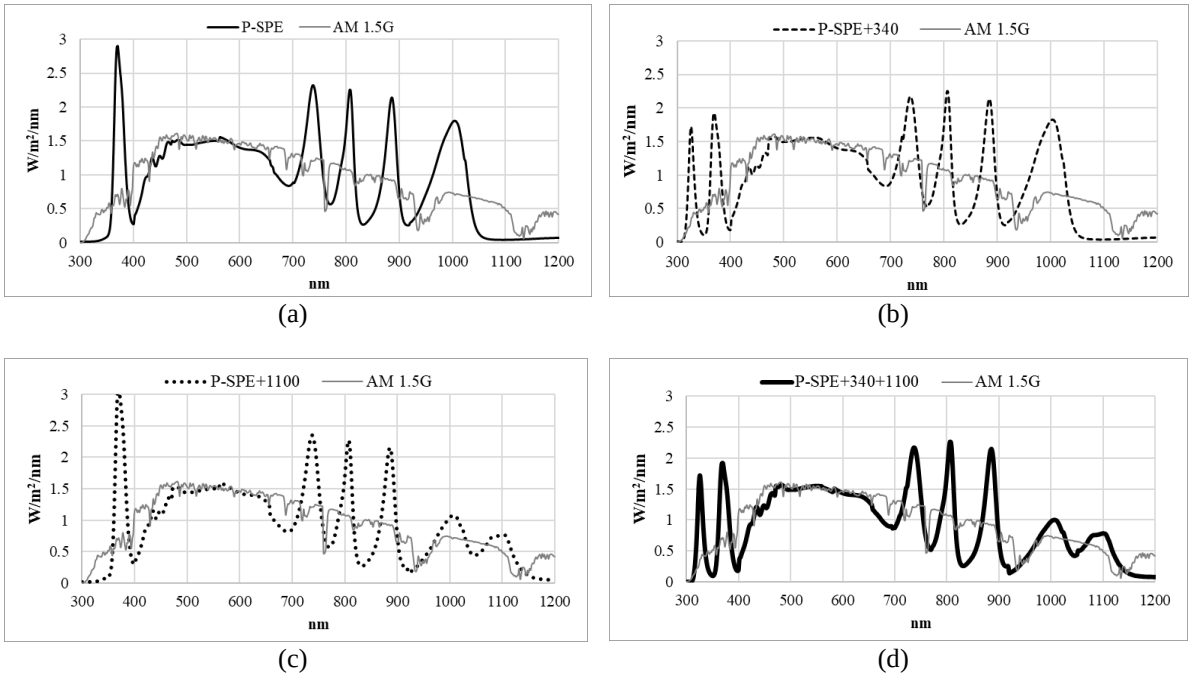

Figure 2. The proposed spectrum distribution: (a) P-SPE (6-types LED; baseline spectrum), (b) P-SPE+340, (c) P-SPE+1100, and (d) P-SPE+ 340+1100

According to Table 2, the spectral match analysis of the P-SPE, as illustrated in Figure 2(a), reveals strong alignment with the AM1.5G reference spectrum across all wavelength ranges. The SM values fall within the Class A+ category (0.938 to 1.073), indicating high accuracy in spectral matching. The overall irradiance power efficiency was 99.44%, corresponding to 833.870 W/m², demonstrating that the total irradiance from the P-SPE closely approximates that of AM1.5G.

Table 2. Characteristics of the P-SPE condition

Wavelength (nm)	AM1.5G (W/m^2)	P-SPE (W/m^2)	SM	Class	SPD (%)	SPC (%)
300–470	140.361	129.804	1.073	A+	36.799	92.962
470–561	138.355	138.385	1.008	A+		
561–657	139.333	148.076	0.938	A+		
657–772	140.236	139.394	0.995	A+		
772–919	140.390	139.602	0.993	A+		
919–1200	139.890	138.608	1.003	A+		
Total	838.564	833.870				

Further analysis of the SPD and SPC, conducted over the wavelength range of 300 to 1,200 nm by IEC 60904-9:2020, showed SPD and SPC values of 36.799% and 92.962%, respectively. The relatively high SPD value (ideal is 0%) indicates minor SPDs, particularly in the 300 to 470 nm and 561 to 657 nm range. Nevertheless, the P-SPE effectively reproduces the energy profile and distribution characteristics of the AM1.5G spectrum. The SPC value of 92.962% confirms that the P-SPE spectrum encompasses a substantial portion of the reference solar irradiance, demonstrating its high suitability for solar simulation applications.

When comparing the P-SPE with the LSS spectrum utilizing six types of LEDs, cool white, 365 nm, 750 nm, 850 nm, 940 nm, and 1,050 nm, as [9], it is evident that P-SPE offers superior performance. The SPD and SPC values of the solar simulator spectrum in [9] were 61.1% and 91.8%, respectively, whereas the P-SPE achieves significantly better results. Additionally, P-SPE outperforms the five-type LSS spectrum used for testing microcrystalline silicon (mc-Si) solar cells in [8], which reported SPD and SPC values of 65.5% and 89.1%, respectively. These differences are reasonable, as the fewer LED types employed in [8] result in insufficient SPC, particularly in the UV and NIR regions, leading to reduced alignment with the standard AM1.5G spectrum and higher SPD.

These findings highlight the effectiveness of the proposed P-SPE as a high-potential irradiance spectrum. Moreover, it presents an opportunity for further optimization to achieve even greater alignment with the AM1.5G standard through the addition of spectral components in the UV and/or NIR regions, as Tables 3 to 5.

Table 3. Characteristics of the P-SPE+340 condition

Wavelength (nm)	AM1.5G (W/m^2)	P-SPE+340 (W/m^2)	SM	Class	SPD (%)	SPC (%)
300–470	140.361	129.988	1.071	A+	34.654	94.176
470–561	138.355	138.367	1.009	A+		
561–657	139.333	148.057	0.938	A+		
657–772	140.236	139.371	0.995	A+		
772–919	140.390	139.573	0.993	A+		
919–1200	139.890	138.552	1.003	A+		
Total	838.564	833.908				

Table 4. Characteristics of the P-SPE+1100 condition

Wavelength (nm)	AM1.5G (W/m^2)	P-SPE+1100 (W/m^2)	SM	Class	SPD (%)	SPC (%)
300–470	140.361	129.804	1.073	A+	28.236	96.284
470–561	138.355	138.385	1.008	A+		
561–657	139.333	148.076	0.938	A+		
657–772	140.236	139.394	0.995	A+		
772–919	140.390	133.882	1.036	A+		
919–1200	139.890	138.801	1.001	A+		
Total	838.564	828.343				

Table 5. Characteristics of the P-SPE+340+1100 condition

Wavelength (nm)	AM1.5G (W/m^2)	P-SPE+340+1100 (W/m^2)	SM	Class	SPD (%)	SPC (%)
300–470	140.361	129.988	1.071	A+	26.088	97.521
470–561	138.355	138.367	1.009	A+		
561–657	139.333	148.057	0.938	A+		
657–772	140.236	139.371	0.995	A+		
772–919	140.390	133.853	1.036	A+		
919–1200	139.890	138.746	1.002	A+		
Total	838.564	828.381				

Table 3 presented the SM results for P-SPE+340 (Figure 2(b)) compared with the standard AM1.5G spectrum. The findings indicate that adding a 340 nm UV component to the baseline P-SPE spectrum enhances its similarity to AM1.5G across all wavelength ranges. The SM values fall within the range of 0.938 to 1.071, placing them within Class A+ according to IEC 60904-9:2020, and demonstrating accuracy

comparable to the original P-SPE. The total irradiance of the P-SPE+340 spectrum was 833.908 W/m², which corresponded to 99.44% of the AM1.5G, indicating a high degree of spectral alignment. The analysis of SPD and SPC over the 300 to 1,200 nm range yielded values of 34.654% and 94.176%, respectively. Although the SPC showed only a slight improvement (~1.2%) over the original P-SPE, the relatively high value suggests that some deviation in spectral shape remains, particularly in the UV region.

Nevertheless, the inclusion of the 340 nm UV LED enhances spectral matching in the UV-sensitive wavelength range (300 to 400 nm), improving energy representation in that region. As a result, the SPC improvement reflects greater overall SPC and suggests that P-SPE+340 offers enhanced conformity to AM1.5G compared to the original P-SPE, while still allowing room for further optimization.

According to Table 4, the P-SPE+1100 spectrum achieved Class A+ SM values (0.938–1.073) with total irradiance reaching 98.78% of AM1.5G, showing strong alignment with the reference. Its SPD and SPC were 28.236% and 96.284%, representing a 3.32–8.56% improvement over the original P-SPE. This highlights the greater impact of adding a single 1,100 nm NIR LED, effectively compensating for the missing 1,050 and 1,200 nm region, compared to the limited contribution of the 340 nm UV LED, which covers only a narrow 50 nm range. Thus, the NIR addition yields broader coverage and a spectrum closer to natural sunlight (300–1,200 nm).

However, when both UV and NIR spectra from 340 nm and 1,100 nm LEDs were added to the P-SPE configuration (Figure 2(d)), the resulting spectrum effectively covered the entire wavelength range from 300 nm to 1,200 nm. The analysis shows that the SM remains within the Class A+, that consistent with previous cases. Although the SM of P-SPE+340+1100 is within acceptable limits, slight deviations are observed in certain wavelength ranges (300 to 470 nm, 561 to 657 nm, as shown in Table 5). It suggests that further spectral tuning may be necessary to ensure uniform spectral balance across the full range. The total irradiance of the P-SPE+340+1100 spectrum reaches 98.79% of the AM1.5G reference value. The SPD and SPC were calculated to be 26.088% and 97.521%, respectively, indicating superior performance compared to all previously examined spectra. In Figure 3, the P-SPE+340+1100 spectrum achieved the lowest SPD and the highest SPC, signifying the highest spectral quality. In contrast, the original P-SPE exhibited the least favorable results, with an SPD of 36.799% and SPC of 92.962%.

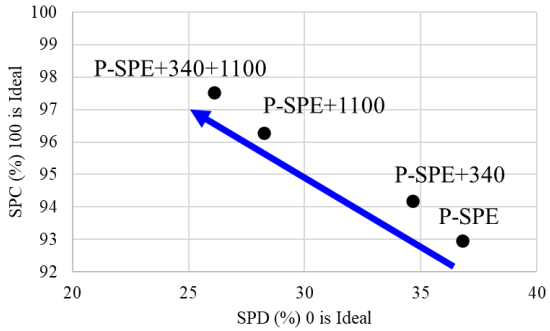

Figure 3. The relationship between SPC and SPD of all the proposed irradiance spectra

These findings confirm that adding only the 1,100 nm NIR LED yields a more significant improvement in spectrum quality than adding the 340 nm UV LED alone. However, combining both UV and NIR enhancements results in the most substantial improvement in spectral performance, maximizing SPC while minimizing SPD. This finding is supported by Yao *et al.* [19], which explains that the output power per unit area of photovoltaic modules illuminated by artificial light sources is significantly lower than that under natural sunlight. This discrepancy is primarily due to differences in spectral distribution, which directly affect the energy conversion efficiency of photovoltaic modules. When comparing the author's optimized spectrum—P-SPE+340+1100 (SPD=26.088% and SPC=97.521%)—with the H8 hybrid spectrum developed by Vosylius *et al.* [8], the advantages in SPD become apparent. The H8 spectrum, which combined seven LEDs (cool white, 365 nm, 405 nm, 523 nm, 740 nm, 850 nm, and 1,050 nm) with a HL for broader NIR coverage, yielded SPD and SPC values of 39.5% and 98.2%, respectively.

Although the difference in SPC between P-SPE+340+1100 and H8 is relatively more (~0.7%), the SPD difference is more substantial (~13%). This larger SPD discrepancy suggests that P-SPE+340+1100 more closely replicates the natural solar spectrum, especially in terms of spectral distribution. Consequently, this difference may significantly affect the accuracy of current output measurements during solar cell testing, as further discussed in the following section.

In summary, selectively adding UV, NIR, or both LEDs improved the P-SPE (6-LED) simulator to Class A+ quality. The 1,100 nm NIR LED had a greater impact on SPD and SPC than UV alone, while combining both best matched the AM1.5G spectrum, achieving up to 98% standard irradiance with minimal LEDs per IEC 60904-9:2020. Beyond spectral optimization, several factors must be addressed for large-scale applications. Thermal management is essential, as LED self-heating can shift peak wavelengths and intensities; adequate cooling ensures long-term spectral stability. Aging and stability also play a role, since LED output gradually degrades over time. Periodic recalibration, in line with IEC 60904-9:2020, is therefore necessary to maintain classification accuracy. Equally important is illumination uniformity, as non-uniform irradiance can distort photovoltaic measurements. Optical diffusers, mixing chambers, or integrating spheres, combined with irradiance mapping, are commonly used to ensure homogeneity within ±2%. Looking ahead, the adoption of broadband white LEDs with extended NIR emission could further reduce SM. The proposed methodology is well-suited to systematically evaluate such emerging sources.

3.2. Impact of spectral deviation and spectral coverage on J_{sc} and J_{ph} of c-Si and mc-Si solar cells

In this study, "photocurrent" (J_{ph}) refers to the simulated current density generated by integrating the solar cell's EQE with the incident spectrum. "Current error" indicates the absolute deviation of J_{ph} or J_{sc} between the proposed LED spectrum and the AM1.5G reference. "Relative error" represents this deviation normalized by the AM1.5G value, expressed as a percentage. These definitions are now clarified in the revised manuscript to avoid ambiguity.The four spectra from section 3.1 were used to simulate their effects on J_{sc} and Jph of c-Si and mc-Si solar cells, as detailed below.

3.2.1. Effect of spectral deviation and spectral coverage on c-Si

The simulated values of J_{sc} and J_{ph} for c-Si solar cells were obtained using four different irradiance spectra with varying SPD and SPC characteristics (Figure 2): P-SPE (6-type LEDs), P-SPE+340, P-SPE+1100, and P-SPE+340+1100. These results were compared against the standard AM1.5G spectrum to evaluate the resulting errors. The analysis outcomes are summarized in Table 6.

Table 6. Simulation results of J_{sc} and J_{ph} for various spectra on a c-Si solar cell

Spectrum	SM	SPC (%)	SPD (%)	AM1.5G		Spectrum		Relative error	
				J_{ph} (mA/cm^2)	J_{sc} (mA/cm^2)	J_{ph} (mA/cm^2)	J_{sc} (mA/cm^2)	J_{ph} (%) error	J_{sc} (%) error
P-SPE	A+	92.962	36.799	46.300	40.460	45.850	43.140	0.956	6.623
P-SPE+340	A+	94.176	34.654	46.300	40.460	45.800	43.050	1.076	6.409
P-SPE+1100	A+	96.284	28.236	46.300	40.460	46.330	41.180	0.069	1.770
P-SPE+340+1100	A+	97.521	26.088	46.300	40.460	46.270	41.090	0.053	1.555

a. Relationship between SPC and current error in c-Si cells

The experimental results indicate that the calculated SPC tended to increase with the addition of spectral sources (e.g., P-SPE+340, P-SPE+1100, and P-SPE+340+1100). The SPC increased from 92.962% in the P-SPE case to 97.521% in the P-SPE+340+1100 case, representing the highest value observed in this study. Additionally, the relative errors in the photovoltaic parameters of the c-Si cell, particularly the J_{ph} and J_{sc}, were found to decrease as SPC increased. This suggests that broader SPC enhances light absorption across a wider wavelength range, resulting in photovoltaic output that more closely matches the standard AM1.5G spectrum. Consequently, the accuracy of the generated current improves, reducing the overall current error.

According to Table 6, the baseline spectrum (P-SPE) exhibited the lowest SPC at 92.962%. Correspondingly, the simulation results showed the highest current errors, with J_{ph} and J_{sc} errors of 0.956% and 6.623%, respectively. Adding only a UV LED at 340 nm slightly increases the SPC by around ~1.2%. While this minor improvement has a positive effect on current accuracy, the reduction in relative error is marginal (less than 0.214%), indicating no significant improvement over the baseline P-SPE. In the case where only the 1100 nm component was added (P-SPE+1100), the SPC showed a considerable improvement, covering 3.32% more of the baseline spectrum. This enhancement also led to a notable reduction in current errors. For instance, the relative error in the J_{sc} decreased to 4.853%, compared to 6.623% in the baseline spectrum. Furthermore, the P-SPE+340+1100 configuration yielded the highest SPC, achieving an SPC of 97.521%. Under this condition, the current errors were minimized, with the J_{ph} and J_{sc} exhibiting the lowest relative errors at 0.053% and 1.555%, respectively. These findings suggest a direct relationship between SPC and the magnitudes of J_{ph} and J_{sc}, and an inverse relationship between SPC and the percentage of current error.

The study confirms that as the SPC of the Class A+ LED irradiance spectrum increases, its coverage extends further into the wavelength range contributing most to current generation. This range is for c-Si's spectral responsivity near 900–1100 nm. This reduces photon flux loss, bringing J_{ph} and J_{sc} closer to AM1.5G values and lowering errors, consistent with [20]. Higher SPC also makes the spectral profile of the test source

more similar to AM1.5G, in line with [21], since J_{ph} is obtained by integrating EQE(λ)×Φphoton(λ) across the spectrum. As SPC increases, Φphoton (λ) aligns more closely with the reference in the EQE-active range, reducing the difference in integrated current and improving agreement of simulated J_{ph} and J_{sc} with AM1.5G.

b. Relationship between SPD and current error in c-Si cells.

The SPD quantifies the deviation in energy distribution between the simulated spectrum and the standard spectrum. As the SPD decreases—indicating higher accuracy in replicating the energy distribution—the error in the current output from the solar cell tends to decrease as well. According to the simulation results (Table 6), the baseline P-SPE, which has an SPD of 36.799% (the highest among the case studies), exhibits relatively high errors (J_{sc} error was 6.623% and J_{ph} error was 0.956%). When the P-SPE is enhanced with the addition of an NIR LED (P-SPE+1100), the SPD decreased to 28.236%, resulting in a substantial reduction in errors of J_{sc} dropped to just 1.770%, and J_{ph} was 0.069%. The best performance was observed when both UV and NIR LEDs were incorporated (P-SPE+340+1100). It reduced the SPD to 26.088% and achieved the lowest current errors, with J_{sc} and J_{ph} errors of 1.555% and 0.053%, respectively. In summary, a lower SPD correlates with improved accuracy in simulating the current response of c-Si solar cells, bringing the simulated values closer to the standard and reducing current measurement errors. A lower SPD of the proposed LED spectrum indicates that its energy distribution more closely matches AM1.5G, preventing redistribution from high-EQE to low-EQE regions. This directly reduces current errors in c-Si cells, consistent with [20], who emphasized that maintaining a solar simulator spectrum close to the reference (low SPD) can significantly improve photovoltaic performance evaluation.

The study reveals that a decrease in the SPD%—from 36.80% in the P-SPE case to 26.09% in the P-SPE+340+1100 case—correlates with a significant reduction in the errors of both J_{ph} and J_{sc}. This SPD reduction indicates that the received spectrum becomes more closely aligned with the standard reference spectrum, thereby enhancing the accuracy of the current generation of solar cells. In summary, high SPC and low SPD indicate better spectral accuracy, leading to reduced errors in J_{ph} and J_{sc}. These metrics are positively correlated with the accuracy of solar cell current evaluation. Thus, spectra with high SPC and low SPD are more suitable for performance testing of photovoltaic cells under IEC 60904-9:2020 standards.

3.2.2. Effect of spectral deviation and spectral coverage on mc-Si

Similarly, the simulated values of J_{sc} and J_{ph} for the mc-Si solar cell were obtained using the same irradiance spectra as in section 3.2.1. The effects of SPD and SPC on mc-Si performance are presented in Table 7. A comparative analysis between the impacts of SPD and SPC on mc-Si (Table 7) and c-Si (Table 6) was illustrated in Figures 4(a)–(d).

Table 7. Simulation results of J_{sc} and J_{ph} for various spectra on a mc-Si solar cell

Spectrum	SM	SPC (%)	SPD (%)	AM1.5G		Spectrum		Relative error	
				J_{ph} (mA/cm^2)	J_{sc} (mA/cm^2)	J_{ph} (mA/cm^2)	J_{sc} (mA/cm^2)	J_{ph} (%) error	J_{sc} (%) error
P-SPE	A+	92.962	36.799	46.300	39.940	45.850	42.680	0.956	5.363
P-SPE+340	A+	94.176	34.654	46.300	39.940	45.800	41.910	1.076	4.933
P-SPE+1100	A+	96.284	28.236	46.300	39.940	46.330	40.720	0.069	1.957
P-SPE+340+1100	A+	97.521	26.088	46.300	39.940	46.270	40.550	0.053	1.524

Based on the analysis of Figures 4(a) and (b), the following key observations can be made: i) effect of SPC percentage on current deviation: For both c-Si and mc-Si solar cells, the SPC approaches 100% and the deviations in both J_{ph} and J_{sc} decrease. This indicates that SPC directly influences the accuracy of current simulation in silicon-based solar cells; ii) comparison between J_{ph} and J_{sc} errors: across all SPC values in both solar cells types, the deviation in J_{sc} (orange dashed line) is consistently higher than that of J_{ph} (blue dashed line). This suggests that J_{sc} is more sensitive to changes in the SPD than J_{ph}; iii) photocurrent comparison between c-Si and mc-Si: the J_{ph} values of c-Si and mc-Si cells show negligible differences across the entire range of SPC values. This observation reflects the fact that both cell types are fabricated from silicon and thus tend to exhibit similar photocurrent characteristics; and iv) short-circuit current error in c-Si vs. mc-Si: When comparing c-Si and mc-Si cells at the same SPC levels, the c-Si cell exhibits higher J_{sc} deviations, particularly in the lower SPC range (≤94%). This can be attributed to the more continuous and purer crystal structure of c-Si, which typically leads to a higher J_{sc} than that of mc-Si [22], [23]. This difference directly contributes to the overall performance variation between the two types of silicon solar cells.

Figures 4(a)–(d) shows that the error values of both c-Si and mc-Si cells decrease as the SPC approaches 100%. In the lower SPC range (~95–96%), however, mc-Si cells exhibit higher errors, indicating greater sensitivity to spectral variations concerning SPC. For SPD, the error increases with increasing values in both cell types, but c-Si cells demonstrate higher errors (up to ~6% compared with ~4% for mc-Si), suggesting a higher susceptibility of c-Si to spectral distortion. The inclusion of error bars (±5%) confirms

that the overall trends remain consistent, and the differences between c-Si and mc-Si remain statistically significant even when uncertainties are considered.

Although the SPC reaches its highest value in the P-SPE+340+1100 configuration, the current density errors in J_{sc} compared to the AM1.5G reference remain at 1.555% for c-Si and 1.524% for mc-Si. This indicates that even with an SPC of 97.521%, the system is still unable to replicate the J_{sc} and J_{ph} values generated under natural sunlight (AM1.5G). Despite the LED-based light source achieving an SPC of 97.521% and an SPD of 26.088% (as shown in Table 7), these values are still noticeably distant from the ideal SPD of 0%. One possible explanation is that LED light emission exhibits discrete spectral peaks, particularly in the UV, deep red, and NIR regions, which may alter the overall photon flux received by silicon solar cells when compares to the continuous AM1.5G spectrum. This SM likely contributes to the observed differences in short-circuit current and photocurrent. This finding is further supported by the previous study on short-circuit current density in silicon solar cells under different spectral light sources [24].

Based on Figures 4(c) and (d), three main findings emerge: i) effect of SPD on current deviation: For both c-Si and mc-Si cells, lower SPD values lead to significantly reduced J_{ph} and J_{sc} deviations, indicating a strong SPD influence on simulation accuracy; ii) J_{ph} vs. J_{sc} errors: across all SPD levels, J_{sc} errors exceed J_{ph} errors, while J_{ph} values remain similar for both cell types, suggesting J_{sc} is more sensitive to SPD changes; and iii) c-Si vs. mc-Si at equal SPD: c-Si cells show greater J_{sc} deviations, especially at ~92% SPD, likely due to their more uniform crystal structure, which reduces internal recombination, and their generally higher EQE from lower electrical losses (series/shunt resistances) [22], enhancing photon-to-carrier conversion and yielding higher J_{sc} [25].

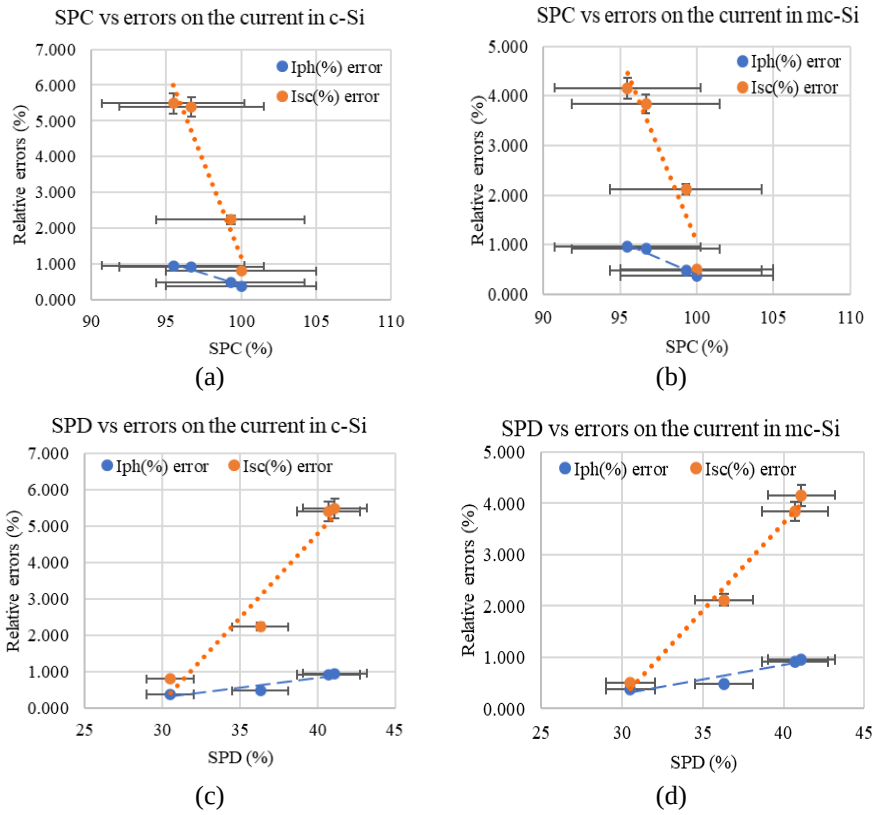

Figure 4. The relationship between SPC and SPD versus current density errors (J_{sc} and J_{ph}) for c-Si and mc-Si solar cells under different LSS spectra; (a) SPC versus current density errors for c-Si, (b) SPC versus current density errors for mc-Si, (c) SPD versus current density errors for c-Si, and (d) SPD versus current density errors for mc-Si

Limitations and sources of deviation persist despite the simulated LED spectrum meeting Class A+. Narrowband peaks, particularly in UV and NIR, cause over-/undershoots and elevated SPD (26–37%), contributing to current errors. The bin-based SM criterion does not fully capture deviations from AM1.5G, and cell-specific spectral sensitivity (c-Si vs. mc-Si) leads to different errors, indicating that EQE(λ)-based spectrum tuning is needed to minimize deviations.

In conclusion, achieving Class A+LSS per IEC 60904-9:2020 requires optimizing SPD and SPC to minimize measurement errors. While J_{ph} remains stable, J_{sc} is sensitive to both SPD and SPC. Incorporating 340 nm (UV) and 1,100 nm (NIR) LEDs enhances accuracy, underscoring the importance of spectral tuning for reliable solar cell testing across different technologies.

4. CONCLUSION

This study demonstrated that enhancing a 6-type LSS (P-SPE) with additional UV (340 nm) and NIR (1,100 nm) LEDs significantly improved its spectral performance. The spectral quality indicators, SPD and SPC, showed that the inclusion of the NIR LED alone offered a greater improvement in both SPD and spectrum coverage compared to UV alone. However, the combination of UV and NIR LEDs yielded the most accurate spectral match to the AM1.5G standard, with total irradiance reaching up to 98.2% of the standard value and achieving Class A+ classification according to IEC 60904-9:2020. Simulation results further confirmed that a higher SPC and a lower SPD corresponded to reduced errors in the calculated short-circuit current density (J_{sc}) and photo-generated current density (J_{ph}) for both c-Si and mc-Si solar cells. The findings indicate that SPD and SPC are reliable indicators for evaluating the spectral accuracy and its impact on current measurement errors. These results suggest that high-quality, LED-based solar simulators can be developed using a minimal number of LEDs while still achieving the spectral criteria required for precise photovoltaic performance testing. Future work may focus on spectral fine-tuning in specific wavelength regions to further minimize deviations and optimize simulator accuracy.

ACKNOWLEDGMENTS

This work was partially supported by Rajamangala University of Technology Suvarnabhumi. We would also like to express our sincere gratitude to photovoltaic lighthouse for providing access to the online Spectral Mismatch Calculator, a valuable tool for simulating spectral data and solar cell currents.

FUNDING INFORMATION

This work was partially supported by Rajamangala University of Technology Suvarnabhumi.

AUTHOR CONTRIBUTIONS STATEMENT

This journal uses the Contributor Roles Taxonomy (CRediT) to recognize individual author contributions, reduce authorship disputes, and facilitate collaboration.

Name of Author	C	M	So	Va	Fo	I	R	D	O	E	Vi	Su	P	Fu
Chaiyant Boonmee	✓	✓		✓	✓	✓		✓	✓	✓			✓	
Patcharanan Sritanauthaikorn	✓	✓	✓	✓	✓			✓	✓	✓	✓			✓
Saichol Chudjuarjeen	✓	✓		✓		✓	✓	✓		✓	✓	✓		
Paiboon Kaitsookkanatorn		✓	✓		✓	✓				✓	✓	✓		
Khanittha Wannakam	✓	✓	✓		✓	✓	✓		✓		✓		✓	✓
Jeerawan Homjan			✓		✓		✓		✓			✓		
Kreeta Sukthang			✓			✓				✓				
Panet Sooksing				✓		✓	✓	✓		✓		✓	✓	
Napat Watjanatepin	✓	✓		✓	✓	✓			✓			✓		✓

C : **C**onceptualization
M : **M**ethodology
So : **So**ftware
Va : **Va**lidation
Fo : **Fo**rmal analysis
I : **I**nvestigation
R : **R**esources
D : **D**ata Curation
O : Writing - **O**riginal Draft
E : Writing - Review & **E**diting
Vi : **Vi**sualization
Su : **Su**pervision
P : **P**roject administration
Fu : **Fu**nding acquisition

CONFLICT OF INTEREST STATEMENT

Authors state no conflict of interest.

INFORMED CONSENT

As this study did not involve the collection of personal information that could identify individuals, informed consent was not applicable.

ETHICAL APPROVAL

As this study did not involve research on humans or animals, the section on ethical approval is not applicable.

DATA AVAILABILITY

Derived data supporting the findings of this study are available from the corresponding author [PS] and [NW] on request.

REFERENCES

[1] A. Younis, P. A. Cotfas, and D. T. Cotfas, "Systematic indoor experimental practices for simulating and investigating dust deposition effects on photovoltaic surfaces: A review," *Energy Strategy Reviews*, vol. 51, 2024, Art. no. 101310, doi: 10.1016/j.esr.2024.101310.

[2] N. Watjanatepin, K. Wannakam, P. Kiatsookkanatorn, C. Boonmee, and P. Sritanauthaikorn, "Improved spectral mismatch and performance of a phosphor-converted light-emitting diode solar simulator," *International Journal of Electrical and Computer Engineering*, vol. 13, no. 5, pp. 4931–4941, 2023, doi: 10.11591/ijece.v13i5.

[3] K. J. Linden, W. R. Neal, and H. B. Serreze, "Adjustable spectrum LED solar simulator," in *Proc. SPIE 9003, Light-Emitting Diodes: Materials, Devices, and Applications for Solid State Lighting XVIII*, Feb. 2014, pp. 109–117, doi: 10.1117/12.2035649.

[4] D. Chojniak *et al*., "A precise method for the spectral adjustment of LED and multi-light source solar simulators," *Progress in Photovoltaics: Research and Applications*, vol. 32, 2024, doi: 10.1002/pip.3776.

[5] International Electrotechnical Commission, *Photovoltaic devices – Part 9: Classification of solar simulator characteristics (IEC 60904-9:2020)*, 2020.

[6] N. Watjanatepin, K. Wannakam, P. Kiatsookanatorn, C. Boonmee, and P. Sritanauthaikorn, "Light sources and irradiance spectrum of LED solar simulator for photovoltaic devices: A review," *International Journal of Renewable Energy Research*, vol. 13, no. 1, pp. 192–207, 2023, doi: 10.20508/ijrer.v13i1.13741.g8675.

[7] International Electrotechnical Commission, *Photovoltaic devices – Part 9: Solar simulator performance requirements (IEC 60904-9:2007)*, 2007.

[8] Ž. Vosylius, A. Novičkovas, and V. Tamošiūnas, "Optimization of LED-based solar simulators for cadmium telluride and microcrystalline silicon solar cells," *Energies*, vol. 16, no. 15, p. 5741, 2023, doi: 10.3390/en16155741.

[9] Ž. Vosylius, D. Antonovic, A. Novickovas, E. Gaubas, and V. Tamosiunas, "Rational selection of light sources for LED-based solar simulators," *Solar Energy*, vol. 265, p. 112064, 2023, doi: 10.1016/j.solener.2023.112064.

[10] N. M. Rada and G. E. Triplett, "Thermal and spectral analysis of self-heating effects in high-power LEDs," *Solid-State Electronics*, vol. 54, no. 4, pp. 378–381, 2010, doi: 10.1016/j.sse.2010.01.016.

[11] N. Watjanatepin and P. Sritanauthaikorn, "Rectangular module for large-scale solar simulator based on high-powered LEDs array," *TELKOMNIKA (Telecommunication Computing Electronics and Control)*, vol. 20, no. 2, pp. 462–474, 2022, doi: 10.12928/telkomnika.v20i2.23308.

[12] H. Lee *et al*., "Performance comparison of tungsten-halogen light and phosphor-converted NIR LED in soluble solid content estimation of apple," *Sensors*, vol. 23, no. 4, p. 1961, 2023, doi: 10.3390/s23041961.

[13] D. Chatterjee and S. Khandekar, "Hybrid solar simulator for long-term testing of photothermal materials," *IEEE Transactions on Instrumentation and Measurement*, vol. 72, pp. 1–8, 2023, Art. no. 3000708, doi: 10.1109/TIM.2023.3295471.

[14] PV Lighthouse, "Spectral mismatch calculator," 2014, [Online]. Available: https://www2.pvlighthouse.com.au/calculators/spectral%20mismatch%20calculator/spectral%20mismatch%20calculator.aspx. (Accessed: Apr. 10, 2025).

[15] M. Meftah *et al*., "A new version of the SOLAR-ISS spectrum covering the 165–3000 nm spectral region," *Solar Physics*, vol. 295, no. 2, pp. 1–16, 2020, doi: 10.1007/s11207-019-1571-y.

[16] Thorlabs, "Light emitting diodes (LEDs)." [Online]. Available: https://www.thorlabs.com/navigation.cfm?guide_id=2101, (Accessed: Jan. 2025).

[17] EPIGAP OSA, "IR LED SMDs," [Online]. Available: https://www.epigap-osa.com/led-smd/ir-smds/. (Accessed: Jan. 2025).

[18] M. A. Green, K. Emery, Y. Hishikawa, W. Warta, and E. D. Dunlop, "Solar cell efficiency tables (version 42)," *Progress in Photovoltaics: Research and Applications*, vol. 21, pp. 827–837, 2013, doi: 10.1002/pip.2404.

[19] W. Yao *et al*., "The impact of spectral distribution on photovoltaic power generation and its quantitative evaluation model," *Applied Energy*, vol. 358, 2024, doi: 10.1016/j.apenergy.2023.122581.

[20] R. Daxini and Y. Wu, "Review of methods to account for the solar spectral influence on photovoltaic device performance," *Energy*, vol. 286, p. 129461, 2024, doi: 10.1016/j.energy.2023.129461.

[21] P. Caprioglio *et al*., "Open-circuit and short-circuit loss management in wide-gap perovskite p-i-n solar cells," *Nature Communications*, vol. 14, no. 932, 2023, doi: 10.1038/s41467-023-36141-8.

[22] M. Green and S. Bremner, "Energy conversion approaches and materials for high-efficiency photovoltaics," *Nature Materials*, vol. 16, pp. 23–34, 2017, doi: 10.1038/nmat4676.

[23] A. Luque and S. Hegedus, *Handbook of Photovoltaic Science and Engineering*. Hoboken, NJ, USA: John Wiley & Sons, 2011, doi: 10.1002/9780470974704.

[24] M. Padilla, B. Michl, B. Thaidigsmann, W. Warta, and M. C. Schubert, "Short-circuit current density mapping for solar cells," *Solar Energy Materials and Solar Cells*, vol. 120, pp. 282–288, 2014, doi: 10.1016/j.solmat.2013.09.019.

[25] M. A. Green, *Silicon Solar Cells: Advanced Principles & Practice*, Centre for Photovoltaic Devices and Systems, 1995.

BIOGRAPHIES OF AUTHORS

Chaiyant Boonmee received his B.Eng. in electrical engineering from Rajamangala Institute of Technology Thewes, his M.Eng. degrees from Rajamangala University of Technology Thanyaburi and his Ph.D. degree in electrical engineering from Chiang Mai University (CMU), Chiang Mai, Thailand, in 2017. His research interests include power electronic application, multilevel cascaded inverters, low cost monitoring system, automation control system, and IoT application. He can be contacted at email: chaiyant.b@rmutsb.ac.th.

Patcharanan Sritanauthaikorn received the B.Eng. (Electrical Engineering) degree from Khon Kaen University, Thailand in 1998, and M.Eng. (Electrical Engineering) degree from King Mongkut's University of Technology Thonburi, Thailand in 2004. Her research interests include control system, automation, power electronics, renewable energy, and LED solar simulator. She can be contacted at email: patcharanan.s@rmutsb.ac.th.

Saichol Chudjuarjeen received the B.Eng. degree from the Mahanakorn University of Technology, Thailand, in 2000, the M.Eng. degree and the Ph.D. degree in electrical and computer engineering from King Mongkut's University of Technology Thonburi, Bangkok, Thailand in 2005 and 2011, respectively. He is an Associate Professor with the Department of Electrical Engineering, Rajamangala University of Technology Krungthep, Bangkok, Thailand. His research interests include high-frequency resonant inverters for induction heating, current-source and voltage-source inverters, renewal energy, green environment, wireless technology, and control of power-electronic systems. He can be contacted at email: saichol.c@mail.rmutk.ac.th.

Paiboon Kiatsookkanatorn received the B.S.Tech.Ed. and B.Eng. degrees from Rajamangala Institute of Technology, Thailand in 1998 and 2002, respectively, and the M.Eng. and Ph.D. degrees from Chulalongkorn University, Bangkok, Thailand in 2005 and 2012, respectively. He is currently an Associate Professor in the Department of Electrical Engineering, Rajamangala University of Technology Suvarnabhumi (RMUTSB), Thailand. His research interests include matrix converters and pulse width-modulation (PWM). He can be contacted at email: Paiboon.k@rmutsb.ac.th.

Khanittha Wannakam received the B.S. in Electrical Engineering from Burapha University, Thailand, in 2007, and the M.S. degree in Electrical Engineering from Chulalongkorn University, Thailand, in 2010, and Ph.D. degree in Electrical Engineering from King Mongkut's Institute of Technology Ladkrabang, Bangkok, Thailand, in 2018. Her research interests are in power system reliability, neural networks in power systems, renewable energy, LED solar simulator, and LED for horticulture and engineering educations. She can be contacted at email: khanittha.w@rmutsb.ac.th.

Jeerawan Homjan received her B.Eng. and M.Eng. degrees in electrical engineering from Suranaree University of Technology (SUT), Thailand, in 2015 and 2019, respectively. In 2020, she was a lecturer in the Department of Mechatronics Engineering, Thaksin University, Phatthalung Campus, Thailand. In 2020, she was a lecturer in the School of Mechatronics Engineering Institute of Engineering, Suranaree University of Technology, Thailand. Since 2022, she has been a lecturer in the Department of Mechatronics Engineering, Faculty of Engineering and Architecture, Rajamangala University of Technology Suvarnabhumi (RMUTSB), Thailand, and since 2024 she has been an Assistant Professor in electrical engineering. Her main research interests include power electronics, control system, motor drive, energy saving, artificial intelligence, applications intelligent, electric vehicle, and LED solar simulator. She can be contacted at email: jeerawan.h@rmutsb.ac.th.

Kreeta Sukthang received the B.Eng., M.Eng., and D.Eng. degrees in Mechanical Engineering from the Faculty of Engineering, King Mongkut's University of Technology Thonburi, Bangkok, Thailand, in 2007, 2009, and 2021, respectively. He has been a Lecturer at the Department of Mechatronics Engineering, Rajamangala University of Technology Suvarnabhumi, Nonthaburi Campus, since 2022. He is currently a research member of the Solar Energy Research and Technology Transfer Center (SERTT). His research interests include finite element analysis (FEA), computational fluid dynamics (CFD), computer-aided design and engineering (CAD/CAE), renewable energy, energy conversion and storage technologies, microscale fluid dynamics, and lab-on-a-chip technologies. He can be contacted at email: kreeta.s@rmutsb.ac.th.

Panet Suksing earned a B.S.Tech.Ed. (Electrical Engineering) degree from Rajamangala University of Technology Thanyaburi in 2006 and an M.Eng. (Electrical Technology) degree Rajamangala University of Technology Thanyaburi in 2013. Power electronics and drives, renewable energy, photovoltaic energy system, and engineering power system are among his research interests. He can be contacted at email: netpoly72@gmail.com.

Napat Watjanatepin earned a B.S.Tech.Ed. (Electrical Engineering) degree from Thailand's Institute of Technology Vocational Education in 1985 and an M.S.Tech.Ed. (Electrical Technology) degree from King Mongkut's Institute of Technology North Bangkok in 1991. Power electronics and drives, renewable energy, photovoltaic energy system, LED solar simulators, LED for horticulture, and engineering education are among his research interests. He won a GOLD MEDAL at iENA 2018 for his invention, "Programmable Spectrum LED Light for Plant Cultivation," and a SILVER MEDAL at the 45th Geneva Innovation Exhibition for the "Six-Spectral LED Solar Simulator." He holds a patent and a petty patent for a total of five inventions. He can be contacted at email: watjanatepin.n@gmail.com.